7. Oligocene–Miocene Terrigenous and Pelagic Sediments, Skiff Bank, Kerguelen Plateau (ODP Leg 183, Site 1139)[1]

Douglas N. Reusch[2]

ABSTRACT

Mixed terrigenous-pelagic sediments from the Oligocene–lower Miocene interval of Hole 1139A accumulated on the flank of an eroded alkalic volcano, Skiff Bank. In this study, I explore relationships among sediment fluxes, especially of organic carbon and the clay mineral byproducts of silicate weathering, and lithologic, tectonic, climatic, and biologic forcing factors. Benthic foraminifers indicate that Skiff Bank had subsided to lower bathyal depths (1000–2000 m) by the Oligocene. Two prominent maxima in noncarbonate concentration at 28 and 22 Ma correspond to peaks in the terrigenous flux; also, high noncarbonate concentrations are associated with larger grain sizes (silt) and higher opal concentrations. These and higher-frequency variations of noncarbonate concentration were probably controlled by glacioeustatic/climatic changes, with higher noncarbonate concentrations caused by increased erosion during glacial lowstands. Around 27 Ma, benthic foraminiferal $\delta^{18}O$ values decreased 0.7‰ as the noncarbonate concentration decreased after the 28-Ma maximum. A paucity of clay-sized sediment and clay minerals suggests that physical erosion, by waves and/or ice, predominated under weathering-limited conditions. Low organic carbon concentrations (~0.13 wt%) also suggest a harsh environment and/or poor preservation in coarse (>2 μm) sediments that were extensively bioturbated below the oxygen minimum zone.

[2] Department of Geological Sciences, 5790 Bryand Global Sciences Center, University of Maine, Orono ME 04469-5790, USA. Present address: Department of Natural Sciences, University of Maine at Farmington, 173 High Street, Farmington ME 04938, USA. **reusch@maine.edu**

INTRODUCTION

Objective 3 of Leg 183 was to determine mass transfer between the volcanic crust and atmosphere-hydrosphere-biosphere system. Basaltic volcanism affects the Earth's climate system, both during the constructive stages, through emission of aerosols and greenhouse gases, and also during the destructive stages, through consumption of carbon dioxide by silicate weathering and organic carbon (OC) burial in volcanogenic sediments (Berner, 1990; Reusch and Maasch, 1998). In large igneous provinces such as the Kerguelen Plateau, these effects may be globally significant. Mafic volcanic rocks contain high concentrations of Ca and Mg silicates and are relatively soluble, making them efficient carbon sinks; chemical denudation rates in basaltic catchments are on the order of 14×10^6 g/km²/yr (1.4 kg/cm²/m.y.) (Bluth and Kump, 1994). Organic carbon burial adjacent to eroding volcanic provinces may also be enhanced because of the large surface area of the layer-silicate weathering products (Mayer, 1994). For example, continental margin sediments contain on the order of 1 mg OC/m² of surface area, and clay-sized fractions yield specific surface areas of 60 m²/g (Bock and Mayer, 2000), so that clay-rich sediments might be expected to contain up to several weight percent OC.

This study contrasts the carbon fluxes associated with erosion of a volcanic terrane (Skiff Bank) with those in the Bengal Fan associated with erosion of middle-crustal sialic material. In the Bengal Fan, organic carbon burial far exceeds carbon sequestration by silicate weathering, in part because of the low concentrations of Ca and Mg silicates in the metamorphic core of the Himalayas and in part because of the highly productive lowlands traversed by the Ganges and Brahmaputra Rivers (France-Lanord and Derry, 1997). In the current study, in addition to measuring the organic carbon flux, I compare the average compositions of terrigenous sediment and volcanic basement to constrain silicate weathering-related carbon dioxide consumption.

An original intent of this study was to characterize weathering of the Kerguelen flood basalt province. At Sites 1136, 1137, and 1138, the tops of subaerially erupted flood basalts are only slightly oxidized, suggesting that little weathering occurred between eruptions. Direct study of weathering profiles at the top of the basement is generally impossible because the regolith has been washed away. (The exception is Broken Ridge, where basalts were pervasively altered to clays following uplift on a rift shoulder and northward translation to a hot and humid climate.)

Site 1139 affords an opportunity to investigate carbon fluxes related to the weathering and erosion of volcanic rocks under variable conditions through the late Oligocene and early Miocene (~30–15 Ma). The site lies in a perched basin on the southwest flank of Skiff Bank, a submerged volcano on the northwest extremity of the Kerguelen Plateau in the southern Indian Ocean (50°11′S, 63°56′E; 1450 m below sea level) (Fig. F1). In Unit II (Shipboard Scientific Party, 2002), volcanogenic materials are mixed with pelagic carbonate, which varies on several scales between 10 and 90 wt%. The bulk of the volcanogenic materials are considered to be terrigenous (i.e., products of terrestrial weathering and erosion) based on presence of clay minerals, predominance of silt, sedimentation rates that are consistent with erosion of a volcanic island, and very rare presence of pyroclastic material such as shards (Shipboard Scientific Party, 2000). Pelagic components record local surface ocean

F1. Bathymetry of the Kerguelen Plateau, p. 14.
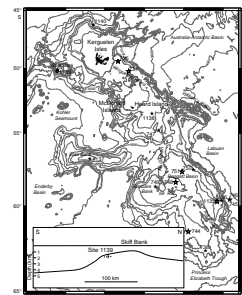
conditions, and benthic foraminifers record bottom conditions including water depth. Ideally, it might be possible to determine how carbon fluxes responded to changing relative sea level and climate. Did increased erosion during glacioeustatic lowstands offset the effect on weathering of low glacial temperatures? How was the organic carbon flux affected by mineral surface area contributed by the terrigenous component?

Hole 1139A cores also bear on the tectonic evolution of the Kerguelen Plateau (Objective 4 of Leg 183) through the Cenozoic. Water depth estimates based on benthic foraminifer assemblages, in combination with glacioeustastic records, are used to reconstruct the subsidence/uplift history of Skiff Bank. The Kerguelen Plateau sits in a critical position with respect to the Antarctic Circumpolar Current (ACC), a major component of the Antarctica–Southern Ocean climate system; in particular, any vertical movements of the plateau may have affected this circulation. Whether or not plateau tectonism affected the ACC, the origin of some carbonate variations in Hole 1139A cores may be rooted in oscillations of this circulation. Unit II sediments potentially contain a detailed record of climate through the Oligocene and Miocene that is analogous to records from other sites receiving mixed terrigenous and pelagic sediment, for example, Ceara Rise near the mouth of the Amazon River (Shackleton, Curry, Richter, and Bralower, 1997) and Site 594 off the east coast of New Zealand (Nelson et al., 1986). At these sites, light oxygen isotopic ratios (interglacials) correspond with high carbonate concentration, high reflectance, and low terrigenous content as indicated by low magnetic susceptibility and low natural gamma activity (and vice versa) (Shackleton, Curry, Richter, and Bralower, 1997; Nelson et al., 1986).

In summary, the major questions posed during this study include

What are the causes of the fluctuations in carbonate concentration?
What is the subsidence/uplift history of Skiff Bank?
What climate signal can be extracted from Hole 1139A cores?
What were the carbon fluxes and how did they respond to changing climate and relative sea level?

ANALYTICAL TECHNIQUES

Two suites of samples were selected, 52 (5-cm^3) samples for geochemical analyses and 35 (20-cm^3) samples for benthic foraminifer studies and stable isotope analyses. The 5-cm^3 samples were chosen to sample the greatest range of variation in the carbonate cycles. The 20-cm^3 samples are spaced at approximately equal time intervals, based on the shipboard biostratigraphy (Shipboard Scientific Party, 2000), and are from carbonate-rich levels.

Calcium carbonate was measured on 52 samples at the University of Rhode Island. Samples were freeze-dried and crushed. Analyses were made with a coulometer on 1-mg aliquots. Two replicates were analyzed per sample, and a third replicate was analyzed when these differed substantially (Table T1). Reported values are the average of the two closest analyses. In addition, estimates of carbonate are based on measurements of reflectance (550 nm) made every 4 cm according to the following logarithmic relationship (Fig. F2) ($R^2 = 0.89$):

T1. Carbon, nitrogen, sulfur, and hydrogen analyses, p. 22.

F2. Reflectance vs. carbonate and grain size, p. 15.
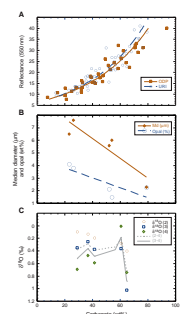
$$CaCO_3 = 43.9 \times \ln (\text{reflectance at 550 nm}) - 81.9. \qquad (1)$$

Organic carbon analyses of 19 samples were made at the University of Maine's Darling Marine Center (Table T1). Aliquots of 30 mg were finely powdered and subjected to HCl fumes to remove carbonate. Organic carbon and nitrogen were measured with a CHN analyzer. A single replicate analysis differs from the first analysis by 0.013 wt% (0.070 and 0.083 wt%). Because of the high carbonate and low OC concentrations, the method of Verardo et al. (1990), which involves dissolving carbonate with sulfurous acid, was attempted on an additional suite of samples. This technique failed when most of the aluminum boats developed holes before the carbonate was entirely dissolved.

Grain size, opal, and major and trace element analyses were conducted on five samples with carbonate ranging from 23 to 79 wt%. Carbonate was first removed with 25% acetic acid (URI/Hovan protocol) on a magnetic stirring hot plate for 2 hr. Samples were centrifuged and rinsed with deionized water three times. Grain sizes were then determined on the decarbonated samples by the X-ray sedigraph method (Table T2). A 0.5% Calgon solution was used to disperse the particles. Afterward, the samples were rinsed with deionized water and centrifuged. Samples were dried at 60°C and weighed. Opal was dissolved with Na_2CO_3 (URI/Hovan protocol). Dried samples were reweighed to determine opal concentrations (Table T2). Major and trace elements were measured on these five samples plus an additional five untreated samples at Washington University by X-ray fluorescence (Table T2).

Five samples with carbonate ranging from 14 to 74 wt% were prepared for X-ray diffraction analyses (Table T3). Carbonate was first removed with weak acetic acid on a magnetic stirring hot plate (Moore and Reynolds, 1997). Samples were rinsed with deionized water and centrifuged. Before size separation, Na phosphate was added to disperse the particles. To separate the clay (<2 μm) fraction, the samples were centrifuged three times until the supernatant cleared. Silt and clay-sized fractions were dried at 60°C. Thin-filter transfers were prepared from the silt fraction. This method did not work for the clay fraction; therefore, smear slides were made. Selective glycolation was used to identify smectite (d-spacing increases from ~15 to >17 Å).

Stable isotope ratios were measured in triplicate on six samples of bulk sediment with carbonate ranging from 29 to 65 wt% (Table T4). Samples were dissolved in phosphoric acid at 90°C and were analyzed at the University of Maine on a VG/Fisons Prism Series II mass spectrometer. Measured ratios were normalized to the Peedee belemnite (PDB) standard according to values of the working standard NBS-20.

The initial 35 plus an additional 23 Oligocene through lower Miocene samples (20 cm³) were prepared for benthic foraminifer studies and stable isotope measurements on the foraminifers. The samples were soaked in a Calgon solution then washed through a 63-μm sieve and dried in an oven at 60°C. Benthic species were separated from the >125-μm fraction in 35 samples and identified by Mimi Katz at Rutgers University (Table T5). The number of specimens retrieved per sample was small, in part because the mostly lithified samples failed to disaggregate despite the Calgon treatment and long duration of soaking. Twenty-three samples yielded sufficient quantities of the benthic foraminifer genera *Cibicidoides* spp. for stable isotope analyses (Table T6). The samples were sonicated to remove matrix material.

Biostratigraphic and paleomagnetic datums used to construct the depth-age plot are shown in Table T7.

RESULTS

Weight Percent CaCO$_3$

Carbonate concentration of the analyzed samples ranges between 7 and 90 wt% (Figs. F2, F3). The mean value is ~50 wt%. The postcruise work shows carbonate variations at three spatial scales: ~100 m, >1 m, and <1 m. The <1-m-scale variations are known only from the proxy reflectance data. These carbonate variations are primary; shipboard descriptions also indicate centimeter-scale through millimeter-scale glauconite laminations that formed during diagenesis (Shipboard Scientific Party, 2000).

Weight Percent Organic Carbon

Organic carbon concentration is generally low (<0.25 wt%) and uniform throughout Hole 1139A (Fig. F3). The mean of organic carbon values is 0.13 wt%. Values range up to 0.35 wt%.

Grain-Size Analyses

Median grain size diameter ranges between 2.3 and 7.6 µm. Smaller sizes are present in the carbonate-rich samples and vice versa (Fig. F2) ($R^2 = 0.83$)

Weight Percent Opal

Opal ranges from 1.5 to 4.1 wt%. The lowest values (~2 wt%) are present in carbonate-rich samples; high values (~4 wt%) are present in carbonate-poor samples (Fig. F2) ($R^2 = 0.62$)

Major and Trace Elements

The average values of major and trace elements in the treated sediments (carbonate and opal removed) are compared with the average values of major and trace elements in the volcanic basement of Skiff Bank in Table T8. Cr and Ni are significantly enriched in the sediments. In a future study, the isocon method should be used to compare the Skiff Bank sediments and basement more rigorously.

Mineralogy (X-Ray Diffraction)

Shipboard X-ray diffraction (XRD) analyses show chlorite in Core 183-1139A-13R (in the upper carbonate minimum) and a trace of smectite in Core 19R (middle carbonate) (Table T3). A sample from Core 183-1139A-27R (lower carbonate minimum; 52 wt% CaCO$_3$) contains a prominent smectite peak. The five samples that were analyzed following decarbonation contain the same assemblage of igneous minerals (plagioclase and sanidine) as identified during shipboard studies (Shipboard Scientific Party, 2000). They do not, however, appear to contain significant amounts of clay minerals.

T7. Depths and ages of faunal, floral, and paleomagnetic criteria, p. 30.

F3. Depth profiles, p. 16.
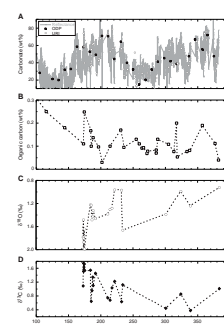
T8. Sediment and basement compositions, p. 31.

Oxygen and Carbon Isotopes

Bulk sediment $\delta^{18}O$ measurements range between 0‰ and ~1‰ (Fig. F2C). They vary considerably in replicate analyses of the same sample (especially low-carbonate samples), and the average values of replicates chosen from a range of carbonate contents are similar (~0.4‰). These values are approximately 1‰ lighter than values from benthic foraminifers, consistent with the bulk sediment being dominated by calcareous nannofossils.

Benthic foraminiferal $\delta^{18}O$ values generally decrease downcore from ~2‰ in Core 183-1139A-19R to <1‰ in Section 40R-CC (Fig. F3). In Core 183-1139A-19R, ratios range between 1.5‰ and 2.0‰. Values <1‰ are present in Cores 183-1139A-24R and 25R, followed by an abrupt downcore increase to >1.6‰.

Benthic foraminiferal $\delta^{13}C$ values range from as high as 1.75‰ in Core 183-1139A-19R to as low as 0.38‰ in Core 36R. They generally decrease downcore, although the value in Section 183-1139A-40R-CC is ~1‰.

Benthic Foraminifer Assemblages

Paleobathymetry at Site 1139 cannot be determined by backtracking because the Kerguelen Plateau has a complex origin and structural evolution (Frey et al., 2000). Benthic foraminifers provide the best tool for reconstructing paleobathymetric history in this setting. Oligocene samples from Hole 1139A yielded too few benthic foraminifers to conduct quantitative analyses of faunal abundance changes. Nonetheless, presence/absence of key depth indicator species yields some paleobathymetric information (M. Katz, pers. comm., 2000).

Species typical of bathyal (200–2000 m) to upper abyssal (2000–3000 m) depths are scattered throughout the Oligocene section recovered from Hole 1139A, including *Astrononion pusillum, Bulimina macilenta, Cibicidoides bradyi, Cibicidoides dickersoni, Cibicidoides eocaenus, Laticarinina pauperata, Melonis barleeanum, Nonion havanense, Osangularia mexicana, Planunlina renzi,* and *Sphaeroidina bulloides.* Species present at Site 1139 that were most common at bathyal depths (200–2000 m) in the Oligocene include *Planulina costata, Planulina renzi, Rectuvigerina multicostata, Uvigerina mexicana,* and *Uvigerina spinulosa. Anomalinoides pseudogrosserugosus* and *Anomalinoides semicribratus* are typically found in Oligocene sediments deposited in water depths >600 m and are present in some samples. *Bulmina impendens* (>500 m; most common at 1000–2000 m) is present throughout, whereas buliminids most common (but not limited to) abyssal depths (>2000 m; *B. glomarchallengeri, B. semicostata,* and *B. grata*) are absent. Similarly, the shallowest species of *Cibicidoides* (*C. crebbsi* and *C. alazanensis*) and deepest species of *Cibicidoides* (*C. havanensis* and *C. lamontdohertyi*) are absent. *Cibicidoides praemundulus* and *Laticarinina pauperata* are most abundant at >1000 m and are found throughout our samples. Benthic foraminiferal species such as *Cibicidoides alazanensis, Neoeponides campester, Rectuvigerina transversa,* and *Siphonina tenuicarinata* that were limited to water depths shallower than 1000 m in the Oligocene are absent from this section. Based on the above depth ranges, we find that the Oligocene section at Site 1139 was deposited at 1000–2000 m depth. Because benthic foraminifers are sparse, it is not possible to speculate on smaller, short-term paleodepth fluctuations based on benthic foraminifers alone.

Benthic foraminiferal assemblages from Site 1139 are similar to those identified for the latest Eocene–Oligocene sections recovered at Kerguelen Plateau Sites 747 and 748 (Schlich, Wise, et al., 1989; Mackensen and Berggren, 1992). Based on benthic foraminifers, Oligocene sediments recovered from Site 747 were deposited at lower bathyal–abyssal depths (>1000 m), and Site 748 was at lower bathyal depths (1000–2000 m) in the Oligocene (Schlich, Wise, et al., 1989).

Chronology

The chronology for Hole 1139A is based on calcareous nannofossils and magnetostratigraphy (Shipboard Scientific Party, 2000) (Fig. F4). Basement $^{40}Ar/^{39}Ar$ age is 68–69 Ma (Duncan, 2002).

The overall sedimentation rate is 23 m/m.y. The depth-age plot (Fig. F4) shows that the sedimentation rate peaked at ~29 and ~22 Ma with a local minimum at ~24 Ma.

DISCUSSION

Sediment Fluxes

Mixed terrigenous-pelagic sediments from Hole 1139A between 150 and 390 meters below seafloor (mbsf) constitute an approximately two-component system. To determine the cause of fluctuations in carbonate concentration, noncarbonate and carbonate fluxes must be calculated independently. The fluxes, or mass accumulation rates (MARs), are determined by multiplying the weight percent of each component, dry bulk density, and sedimentation rate. For example:

$$CaCO_3 \text{ MAR} = \text{wt\% } CaCO_3 \times \text{dry bulk density} \times \text{sedimentation rate}, \quad (2)$$

where,
MAR = g/cm²/m.y.,
wt% $CaCO_3$ = g $CaCO_3$/g sediment,
bulk density = g/cm³, and
sedimentation rate = cm/m.y.

Thus, the resolution of the depth-age curve (Fig. F4) strongly influences the flux estimates. Also, the low age resolution prohibits making flux estimates at the shorter timescales that correspond to the second- and third-order carbonate variations.

Carbonate accumulation rate varied only slightly at Site 1139 (Fig. F5A). It reached >2 kg/cm²/m.y. in the late early Oligocene (~30 Ma) and gradually fell to <1 kg/cm²/m.y. in the Miocene.

The two prominent minima in carbonate concentration at 100–160 and 250–290 mbsf (Fig. F3) correspond to high sedimentation rates and peaks in the noncarbonate flux. Specifically, noncarbonate accumulation peaked at >3 kg/cm²/m.y. at ~29 Ma, decreased to <1 kg/cm²/m.y. between 26 and 23 Ma, peaked at >4 kg/cm²/m.y. at ~22 Ma, and became minimal by 21 Ma (Fig. F5B). Hence, variable terrigenous input is largely responsible for the long-term variation of carbonate concentration in Hole 1139A cores.

The flux of clay minerals from Skiff Bank to the Site 1139 basin is judged to have been limited because the terrigenous fraction is mostly silt sized (Fig. F2B). The magnetic susceptibility record and magnetic

F4. Age-depth plot, p. 18.
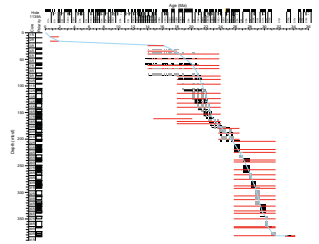
F5. Fluxes of carbonate, noncarbonate, and organic carbon, p. 19.
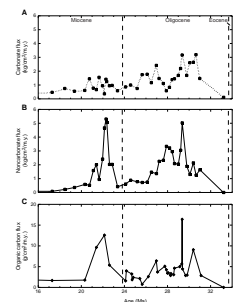
grains observed during sample preparation also indicate that the terrigenous component is relatively coarse (>2 µm). Although the shipboard X-ray diffraction results list clay minerals, clay minerals were not prominent in XRD analyses of decarbonated samples of this study (Table T3). Whole-rock elemental analyses also suggest a predominance of igneous (i.e., unweathered) material in the terrigenous component (Table T8).

The flux of organic carbon at Site 1139 was ~5 g/cm²/m.y. (Fig. F5C). This falls at the low end of the range of carbon fluxes from different settings around the world including surficial pelagic sediments from the open oceans (Berner, 1982).

Lithology of Source Area

Lithology was most likely constant through the history of weathering and erosion of Skiff Bank. Ideally for the purposes of this study, the provenance of Skiff Bank sediments would be uniform flood basalts. Skiff Bank basement, however, comprises evolved alkaline materials, including trachytic basalts, trachytes, and even rhyolites. Volcanic and hydrothermal features indicate that erosion did not progress to a deep level in the basement at Site 1139 (Shipboard Scientific Party, 2000). There is no indication of a change in provenance through this interval as indicated by the gross mineralogy of the sediments (Table T3).

Relative Sea Level

Despite small numbers of specimens compared to Leg 120 studies, the quality of our benthic foraminifer data is as good. The lack of significant variation indicates that any changes in relative sea level were not large enough to be recognized by this technique, which places Site 1139 in the lower bathyal zone (1000–2000 m) throughout the Oligocene and Miocene Epochs.

The nannofossil *Braarudosphaera bigelowii* (Sample 183-1139A-30R-CC) is normally a neritic taxon (Shipboard Scientific Party, 2000). Its occurrence, which coincides with the peak of terrigenous sedimentation rate at ~29 Ma, affords weak evidence for a minimum in water depth at this time. Possibly, the erosional pulse correlates with the mid-Oligocene glacioeustatic sea level fall TB1.1 and subsequent lowstand (Haq et al., 1987) and oxygen isotopic zone Oi2 (e.g., Pekar and Miller, 1996).

Subsidence and Tectonic Forcing

The subsidence and uplift history of Skiff Bank is constrained by benthic foraminifers (Fig. F6). An unexpectedly old basement age of 68–69 Ma (Duncan, 2002) suggests that the majority of subsidence occurred in the early Paleogene. The lack of variation in benthic foraminifers is consistent with Skiff Bank lithosphere having stabilized by the Oligocene (~35 m.y. later).

Skiff Bank lies ~350 km from the Kerguelen archipelago (Fig. F1). Flood basalt activity on the archipelago peaked at ~25 Ma (Nicolaysen et al., 2000) (Fig. F6) when the terrigenous sedimentation rate at Skiff Bank reached a minimum (Fig. F5B). This broad temporal coincidence suggests a possible connection through depression of the lithosphere around the thick pile of flood basalts that accumulated to form the archipelago. This connection, however, is considered dubious because the peripheral forebulge around Hawaii has a similar radius but Hawaii is

F6. Basement elevation and rate of flood basalt eruption, p. 20.
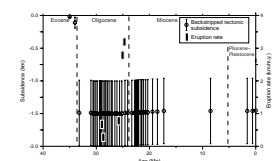
built on relatively old, thick lithosphere; most likely, Skiff Bank lies too far from the Kerguelen archipelago to have been affected by plume activity during the Oligocene.

Biologic and Climatic Forcing

A bloom of the nannofossil *Braarudosphaera bigelowii* (Sample 183-1139A-30R-CC) suggests biologic forcing in the mid-Oligocene (Shipboard Scientific Party, 2000) and possibly contributed to the slightly higher carbonate accumulation rates between ~31 and ~27 Ma (Fig. F5A). This event, however, cannot account for the subsequent relatively high carbonate concentrations between ~27 and ~23 Ma (Fig. F7A), a time when the carbonate accumulation rate was relatively slow and constant (<2 kg/cm²/m.y.) (Fig. F5A). Hence, high biological productivity is not a likely cause of the high carbonate concentrations in the latest Oligocene.

We have few direct constraints on the local climate at Site 1139. Surficial conditions, however, may be inferred from our oxygen isotopic analyses on benthic foraminifers from Hole 1139A (Fig. F7B) and by correlating with more detailed records from other sites. In particular, the detailed records indicate a prominent late Oligocene warming at around 26 Ma and a glaciation at the beginning of the Miocene (just before 23.0 Ma) (Zachos et al., 2001). A future study should explore an age model that correlates our downhole increase in $\delta^{18}O$ from 0.97‰ (232.10 mbsf) to 1.66‰ (233.88 mbsf) with the 26-Ma warming event and our downhole decrease from 1.99‰ (175.03 mbsf) to 1.22‰ (184.04 mbsf) with the 23-Ma cooling event.

An important aspect of climate often forgotten is wind strength. Considering that Skiff Bank may have been a small island in a large ocean, variable wind speed and wave intensity through climate cycles may have been very significant in determining the erosional history of the coastline.

Variations of Noncarbonate

Carbonate productivity and tectonic factors are less likely to have controlled the variations of noncarbonate concentration at Site 1139 than glacioeustatic sea level and climate changes. First, on a multimillion-year timescale, the coincidence of high noncarbonate concentration and fast sedimentation rate indicates that carbonate was diluted (Figs. F3, F4); this relationship might extend to shorter timescales. Second, grain sizes increase with increasing noncarbonate (Fig. F2B), suggesting that the gradational boundary between terrigenous and pelagic facies shifted basinward during lowstands of sea level. Third, opal concentration increases with increasing noncarbonate (Fig. F2B), which is consistent with latitudinal shifting of the gradational facies boundary between cold-water silica-rich sediments and warm-water carbonate-rich sediments. (Alternatively, opal may partially dissolve in carbonate-rich sediment due to higher pH.) Fourth, the carbonate pattern resembles the glacioeustatic record (Zachos et al., 2001). Fifth, the setting of Site 1139 resembles that of other sites of mixed terrigenous-pelagic sedimentation (e.g., Site 594 and Ceara Rise), where noncarbonate tracks the benthic foraminifer oxygen isotope record (low carbonate during glacials is attributed to dilution by terrigenous sediments).

In the carbonate-rich intervals, intermediate (>1 m) cycles may correlate with million-year to 400-k.y. cycles identified in oxygen isotope

F7. Time series for the period 34–20 Ma, p. 21.
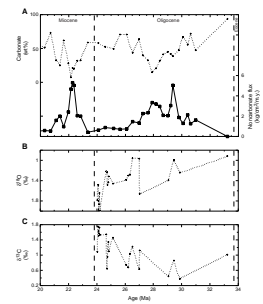
and continental margin studies (Oi and Mi events of Miller et al., 1991). The highest frequency cycles may be 40 k.y. in duration, which are conspicuous in Ceara Rise sediments that accumulated at a similar rate (Zachos et al., 2001).

Implications for Atmospheric Carbon Dioxide

How did silicate weathering vary and respond to environmental changes at Skiff Bank? The paucity of clay minerals and clay-sized sediments indicates that physical weathering and erosion were dominant (i.e., weathering-limited regime of Stallard and Edmond, 1983) and possibly that consumption of atmospheric carbon dioxide by silicate weathering was minimal (although this flux is high in Iceland, where high rainfall and mechanical breaking of rocks compensate for the low temperatures) (Gislason et al., 1996).

The organic carbon concentrations are low and relatively constant (Fig. F5C). The likely causes include minimal terrigenous OC production in a cold, hostile climate and poor preservation in coarse sediments with low mineral surface area that were extensively burrowed at a depth below the oxygen minimum layer.

A crude comparison between Skiff Bank and Himalayan carbon fluxes can now be made. Carbon dioxide consumption related to silicate weathering is unlikely to have been excessive at either location, at Skiff Bank because of limited weathering and in the Himalayan system because of inappropriate materials (paucity of soluble Ca- and Mg-silicates) (France-Lanord and Derry, 1997). The organic carbon flux at Skiff Bank (~5 g/cm²/m.y.) is minor compared to the Bengal Fan, where long-term sedimentation rates are triple and OC concentrations are up to an order of magnitude greater (France-Lanord and Derry, 1994).

CONCLUSIONS

Skiff Bank accomplished most of its subsidence prior to the Oligocene and had stabilized by 32 Ma. Skiff Bank is probably too remote from the Kerguelen archipelago to have been affected by plume activity there during the Oligocene.

Noncarbonate variations are large (10–90 wt%) at the ~100-m scale. Additional analyses show intermediate-scale (>1 m) variations up to 40 wt%, and reflectance measurements show previously unrecognized small-scale (<1 m) variations up to 20 wt%.

Carbonate concentration probably reflects glacioeustatic sea level and/or climate changes because it varies inversely with sedimentation rate, grain size, and opal concentration and by analogy with similar mixed terrigenous-pelagic sequences where relatively constant carbonate input was diluted by terrigeneous sediment during glacials. Specifically, the large mid-Oligocene terrigenous pulse at Site 1139 may correlate with a glacioeustatic lowstand (TB1.1 of Haq et al., 1987; Oi2 of Miller et al., 1991); the late Oligocene period of low terrigenous flux follows a large decrease in benthic foraminiferal $\delta^{18}O$; and the early Miocene terrigenous pulse follows an increase in benthic foraminiferal $\delta^{18}O$ near the Oligocene/Miocene boundary.

Low organic carbon concentrations (and fluxes) throughout the Oligocene and early Miocene are attributed to a hostile terrestrial environment, lack of mineral surface area (predominance of silt), and

deposition followed by extensive bioturbation below the oxygen minimum zone.

Although silicate weathering is high in comparable modern settings (southwestern Iceland), a paucity of clay minerals and clay-sized sediment (and presence of primary igneous minerals and predominance of silt) suggests that physical processes dominated over chemical weathering. It is likely that Skiff Bank was attacked by waves and perhaps was eroded by ice during the Oligocene and early Miocene. Site 1139 is a strategic site because of the intercalated terrigenous and pelagic components. The cores, however, are difficult to work with; specifically, the microfossil components are both difficult to extract from lithified material and difficult to clean.

ACKNOWLEDGMENTS

REFERENCES

Berggren, W.A., Kent, D.V., Swisher, C.C., III, and Aubry, M.-P., 1995. A revised Cenozoic geochronology and chronostratigraphy. *In* Berggren, W.A., Kent, D.V., Aubry, M.-P., and Hardenbol, J. (Eds.), *Geochronology, Time Scales and Global Stratigraphic Correlation.* Spec. Publ.—SEPM (Soc. Sediment. Geol.), 54:129–212.

Berner, R.A., 1982. Burial of organic carbon and pyrite sulfur in the modern ocean: its geochemical and environmental significance. *Am. J. Sci.,* 282:451–473.

————, 1990. Atmospheric carbon dioxide levels over Phanerozoic time. *Science,* 249:1382–1386.

Bluth, G.J.S., and Kump, L.R., 1994. Lithologic and climatologic controls of river chemistry. *Geochim. Cosmochim. Acta,* 58:2341–2359.

Bock, M.J., and Mayer, L.M., 2000. Mesodensity organo-clay associations in a near-shore sediment. *Mar. Geol.,* 163:65–75.

Duncan, R.A., 2002. A time frame for construction of the Kerguelen Plateau and Broken Ridge. *J. Petrol.,* 43:1121–1137.

France-Lanord, C., and Derry, L.A., 1994. $\delta^{13}C$ of organic carbon in the Bengal Fan: source evolution and transport of C_3 and C_4 plant carbon to marine sediments. *Geochim. Cosmochim. Acta,* 58:4809–4814.

————, 1997. Organic carbon burial forcing of the carbon cycle from Himalayan erosion. *Nature,* 390:65–67.

Frey, F.A., Coffin, M.F., Wallace, P., Weis, D., and Leg 183 Shipboard Scientific Party, 2000. Origin and evolution of a submarine large igneous presence: the Kerguelen Plateau and Broken Ridge, southern Indian Ocean. *Earth Planet. Sci. Lett.,* 176:73–89.

Gislason, S.R., Arnorsson, S., and Armannsson, H., 1996. Chemical weathering of basalt in southwest Iceland: effects of runoff, age of rocks and vegetative/glacial cover. *Am. J. Sci.,* 296:837–907.

Haq, B.U., Hardenbol, J., and Vail, P.R., 1987. Chronology of fluctuating sea levels since the Triassic. *Science,* 235:1156–1167.

Mackensen, A., and Berggren, W.A., 1992. Paleogene benthic foraminifers from the southern Indian Ocean (Kerguelen Plateau): biostratigraphy and paleoecology. *In* Wise, S.W., Jr., Schlich, R., et al., *Proc. ODP, Sci. Results,* 120: College Station, TX (Ocean Drilling Program), 603–630.

Mayer, L.M., 1994. Relationships between mineral surfaces and organic carbon concentrations in soils and sediments. *Chem. Geol.,* 114:347–363.

Miller, K.G., Wright, J.D., and Fairbanks, R.G., 1991. Unlocking the Ice House: Oligocene–Miocene oxygen isotopes, eustasy, and margin erosion. *J. Geophys. Res.,* 96:6829–6848.

Moore, D.M., and Reynolds, R.C., 1997. *X-Ray Diffraction and the Identification and Analysis of Clay Minerals* (2nd ed.): Oxford (Oxford Univ. Press).

Nelson, C.S., Hendy, C.H., Cuthbertson, A.M., and Jarrett, G.R., 1986. Late Quaternary carbonate and isotope stratigraphy, subantarctic Site 594, Southwest Pacific. *In* Kennett, J.P., von der Borch, C.C., et al., *Init. Repts. DSDP,* 90: Washington (U.S. Govt. Printing Office), 1425–1436.

Nicolaysen, K., Frey, F.A., Hodges, K.V., Weis, D., and Giret, A., 2000. $^{40}Ar/^{39}Ar$ geochronology of flood basalts from the Kerguelen archipelago, southern Indian Ocean: implication for Cenozoic eruption rates of the Kerguelen plume. *Earth Planet. Sci. Lett.,* 174:318–328.

Pekar, S.F., and Miller, K.G., 1996. New Jersey Oligocene "Icehouse" sequences (ODP Leg 150X) correlated with global $\delta^{18}O$ and Exxon eustatic records. *Geology,* 24:567–570.

Reusch, D.N., and Maasch, K.A., 1998. The transformation from arc volcanism to exhumation, weathering of young Ca, Mg, and Sr silicates, and CO_2 drawdown. *In*

Crowley, T.J., and Burke, K.C. (Eds.), *Tectonic Boundary Conditions for Climate Reconstructions:* New York (Oxford Univ. Press), 261–276.

Schlich, R., Wise, S.W., Jr., et al., 1989. *Proc. ODP, Init. Repts.,* 120: College Station, TX (Ocean Drilling Program).

Shackleton, N.J., Curry, W.B., Richter, C., and Bralower, T.J. (Eds.), 1997. *Proc. ODP, Sci. Results,* 154: College Station, TX (Ocean Drilling Program).

Shipboard Scientific Party, 2000. Site 1139. *In* Coffin, M.F., Frey, F.A., Wallace, P.J., et al., *Proc. ODP, Init. Repts.,* 183, 1–213 [CD-ROM]. Available from: Ocean Drilling Program, Texas A&M University, College Station, TX 77845-9547, U.S.A.

Stallard, R.F., and Edmond, J.M., 1983. Geochemistry of the Amazon, 2: the influence of geology and weathering environment on the dissolved load. *J. Geophys. Res.,* 88:9671–9688.

Verardo, D.J., Froelich, P.N., and McIntyre, A., 1990. Determination of organic carbon and nitrogen in marine sediments using the Carlo Erba NA-1500 Analyzer. *Deep-Sea Res. Part A,* 37:157–165.

Zachos, J.C., Shackleton, N.J., Revenaugh, J.S., Pälike, H., and Flower, B.P., 2001. Climate response to orbital forcing across the Oligocene-Miocene boundary. *Science,* 292:274–278.

Figure F1. Bathymetry of the Kerguelen Plateau. Contour interval = 500 m. Inset is a schematic north-south cross section through Site 1139. The dashed line indicates contact between sediments and volcanic basement.
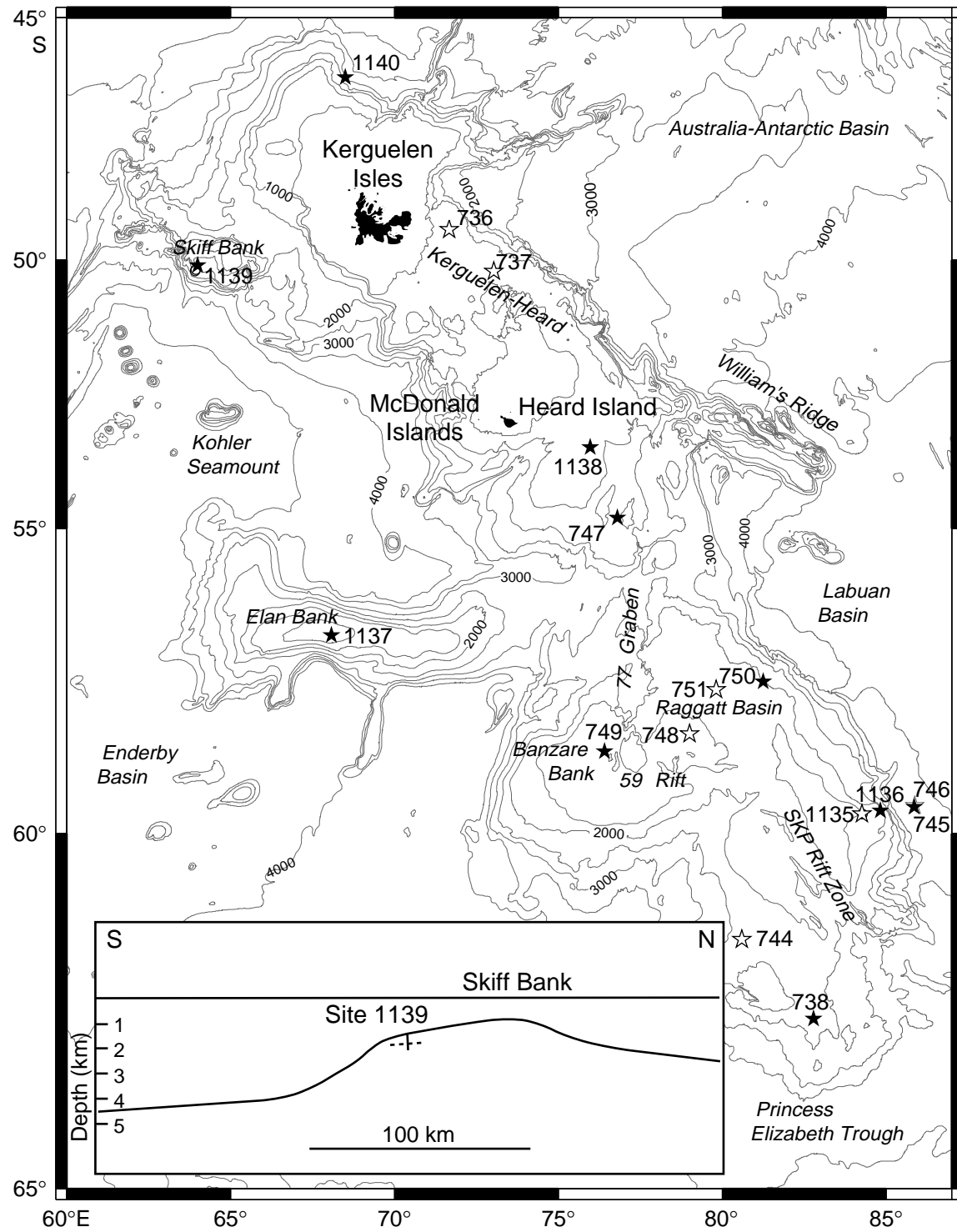
Figure F2. A. Reflectance vs. carbonate analyzed by coulometer method. ODP = Ocean Drilling Program. URI = University of Rhode Island. **B.** Median grain size diameter and opal vs. carbonate; linear regressions are $-0.0787 \times CaCO_3 = 9.2824$ ($R^2 = 0.83$) and $-0.0391 \times CaCO_3 + 4.5917$ ($R^2 = 0.62$), respectively. **C.** Bulk sediment $\delta^{18}O$ vs. carbonate; (2), (3), and (4) are replicate analyses; lines are mean values.
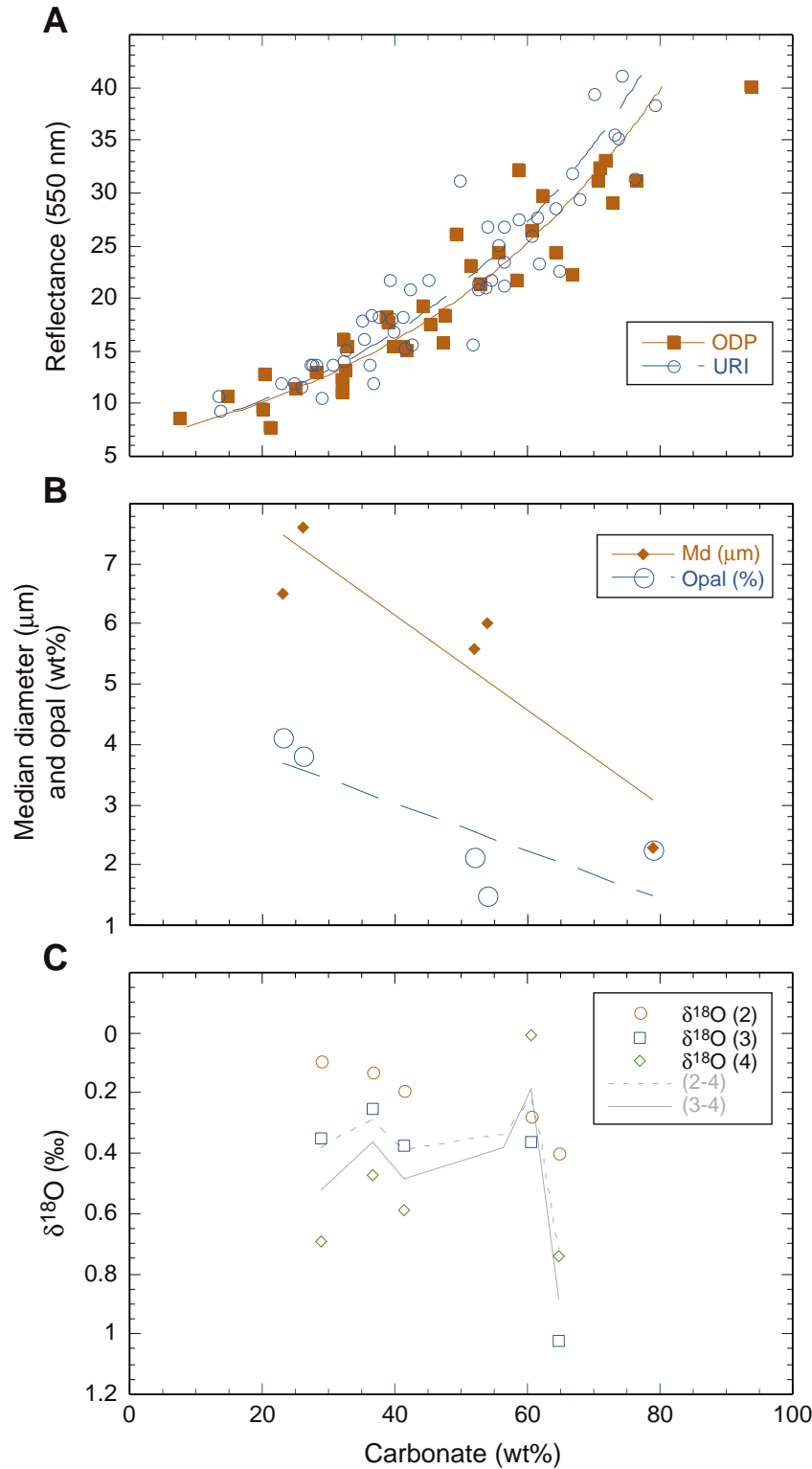
Figure F3. Depth profiles, Site 1139. **A.** Bulk $CaCO_3$ contents. The gray line is carbonate estimated from reflectance data using equation 1. ODP = Ocean Drilling Program. URI = University of Rhode Island. **B.** Organic carbon. **C.** $\delta^{18}O$ measured on benthic foraminifers. **D.** $\delta^{13}C$ measured on benthic foraminifers. (Continued on next page.)
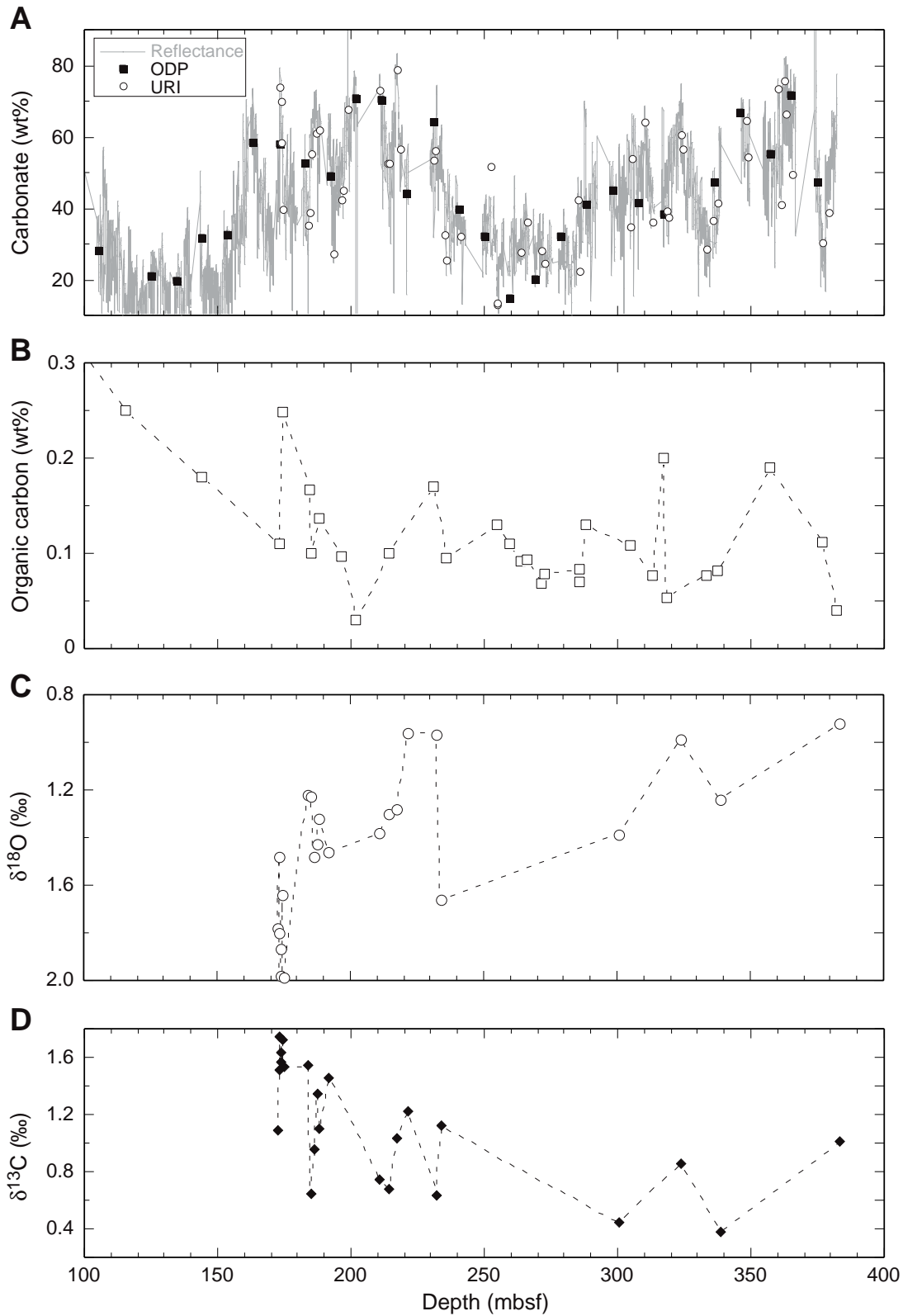
Figure F3 (continued). E. A high-resolution view of a portion of the carbonate data presented in A.
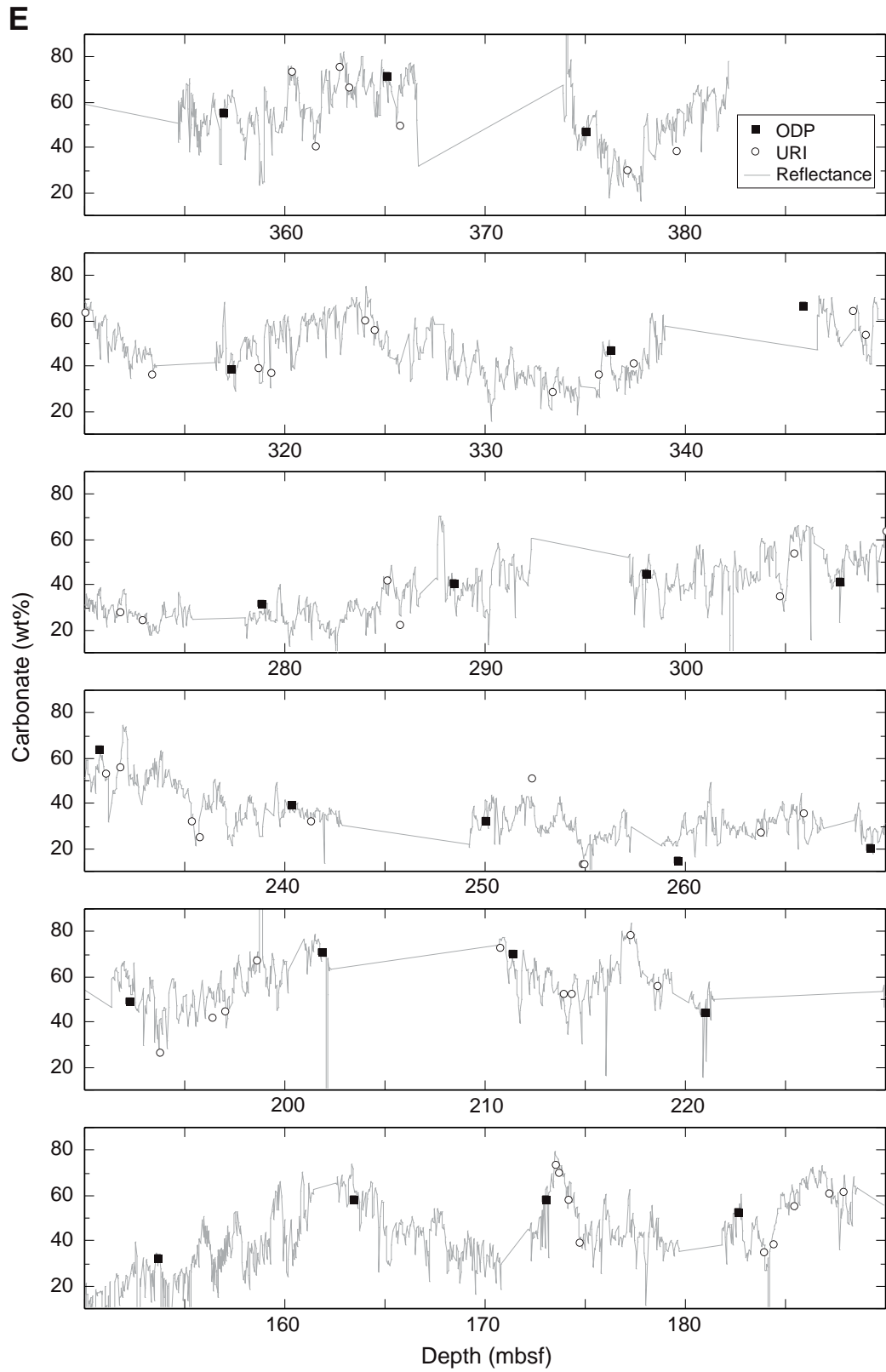
Figure F4. Age-depth plot for Site 1139 (graph provided by F. Boehm). The first time derivative shows peaks in sedimentation rate at ~29 and ~22 Ma.
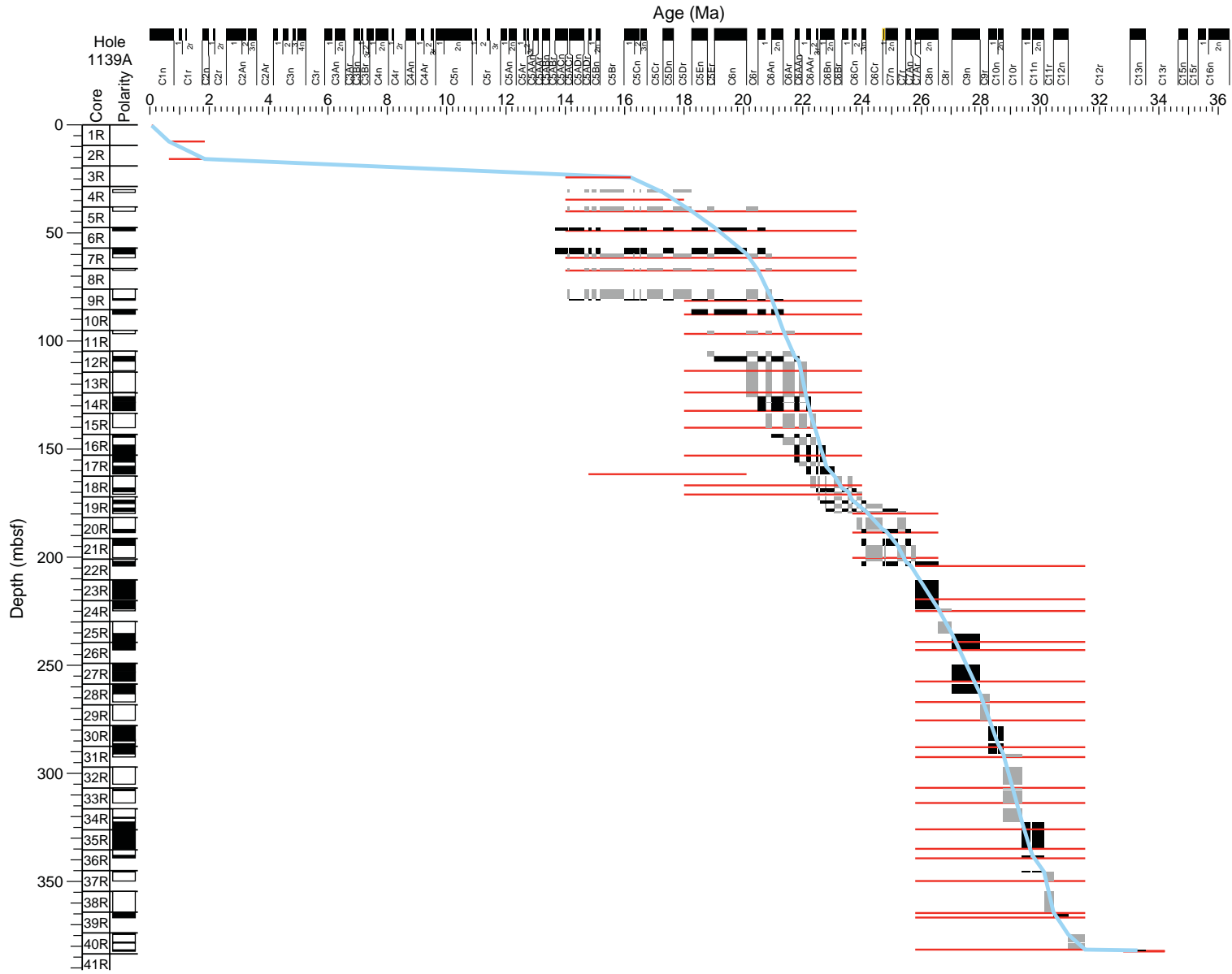
Figure F5. Fluxes of (**A**) carbonate, (**B**) noncarbonate, and (**C**) organic carbon plotted vs. age (34–16 Ma) calculated using equation 2. Sedimentation rates were calculated based on the age-depth relationships shown in Figure F4, p. 18.
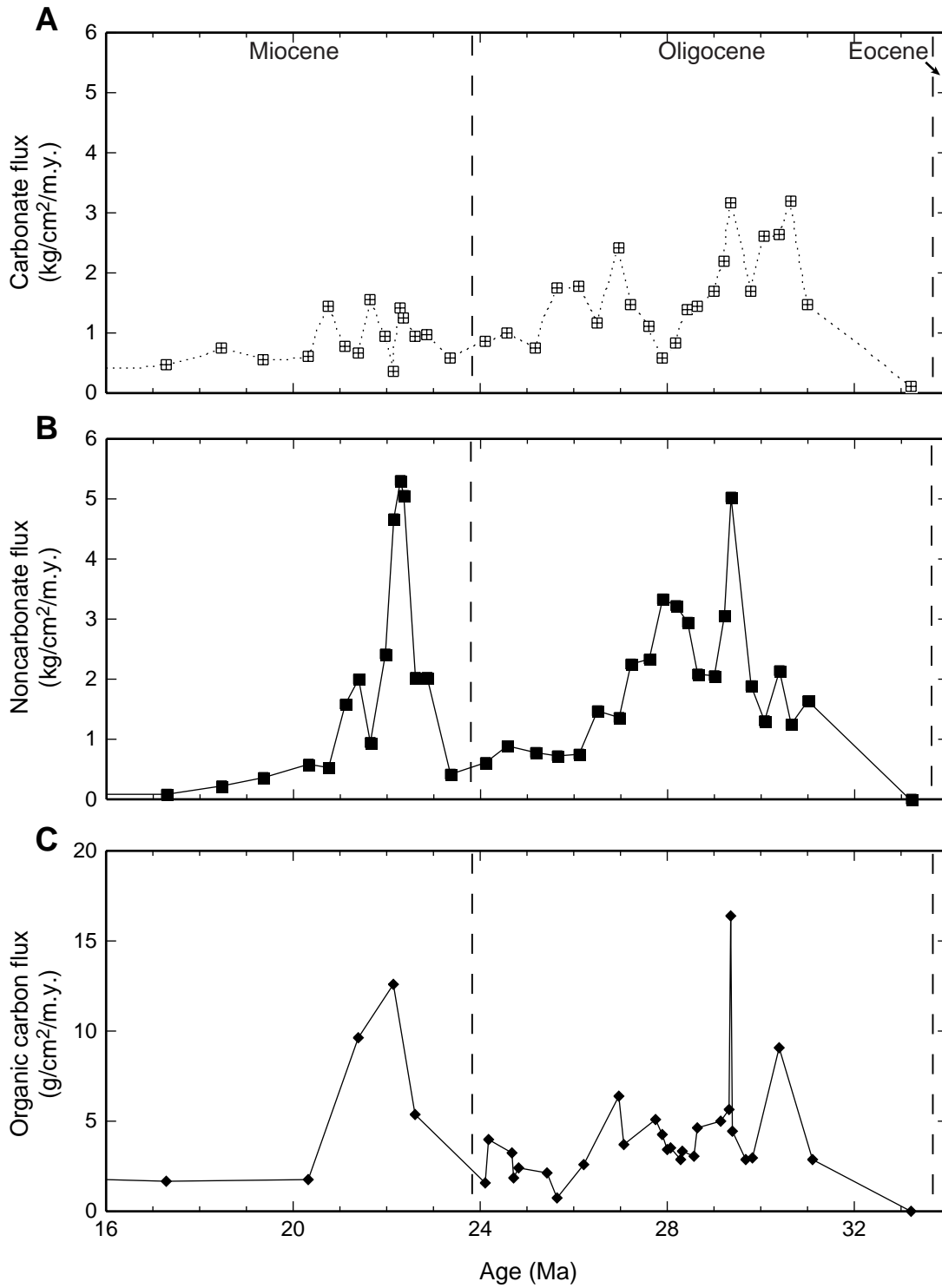
Figure F6. Basement elevation and rate of flood basalt eruption at the Kerguelen archipelago plotted vs. age (40–0 Ma). Backstripped tectonic subsidence was provided by D. Muller using the paleodepth estimates of M. Katz presented in this paper. Eruption rates are calculated from data presented in Nicolaysen et al. (2000).
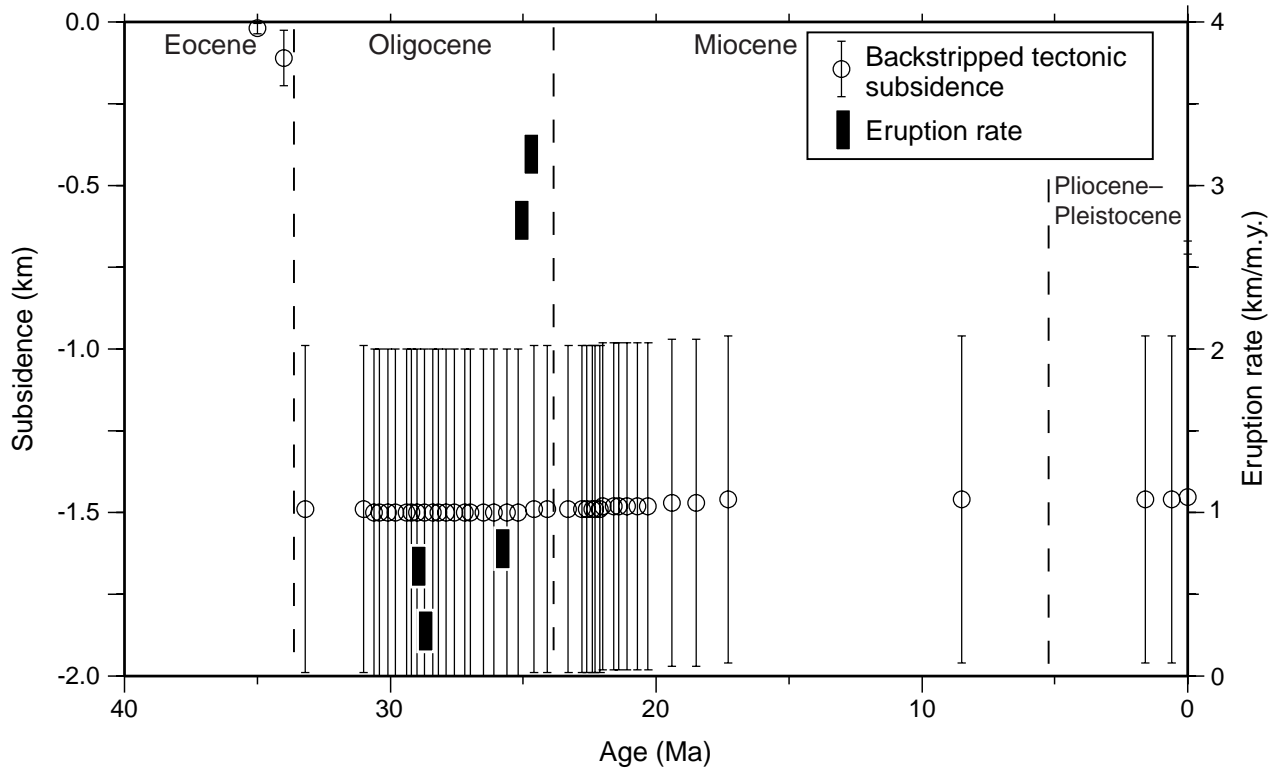
Figure F7. Time series of (**A**) carbonate and noncarbonate flux, (**B**) benthic foraminiferal $\delta^{18}O$, and (**C**) benthic foraminiferal $\delta^{13}C$ for the period 34–20 Ma.
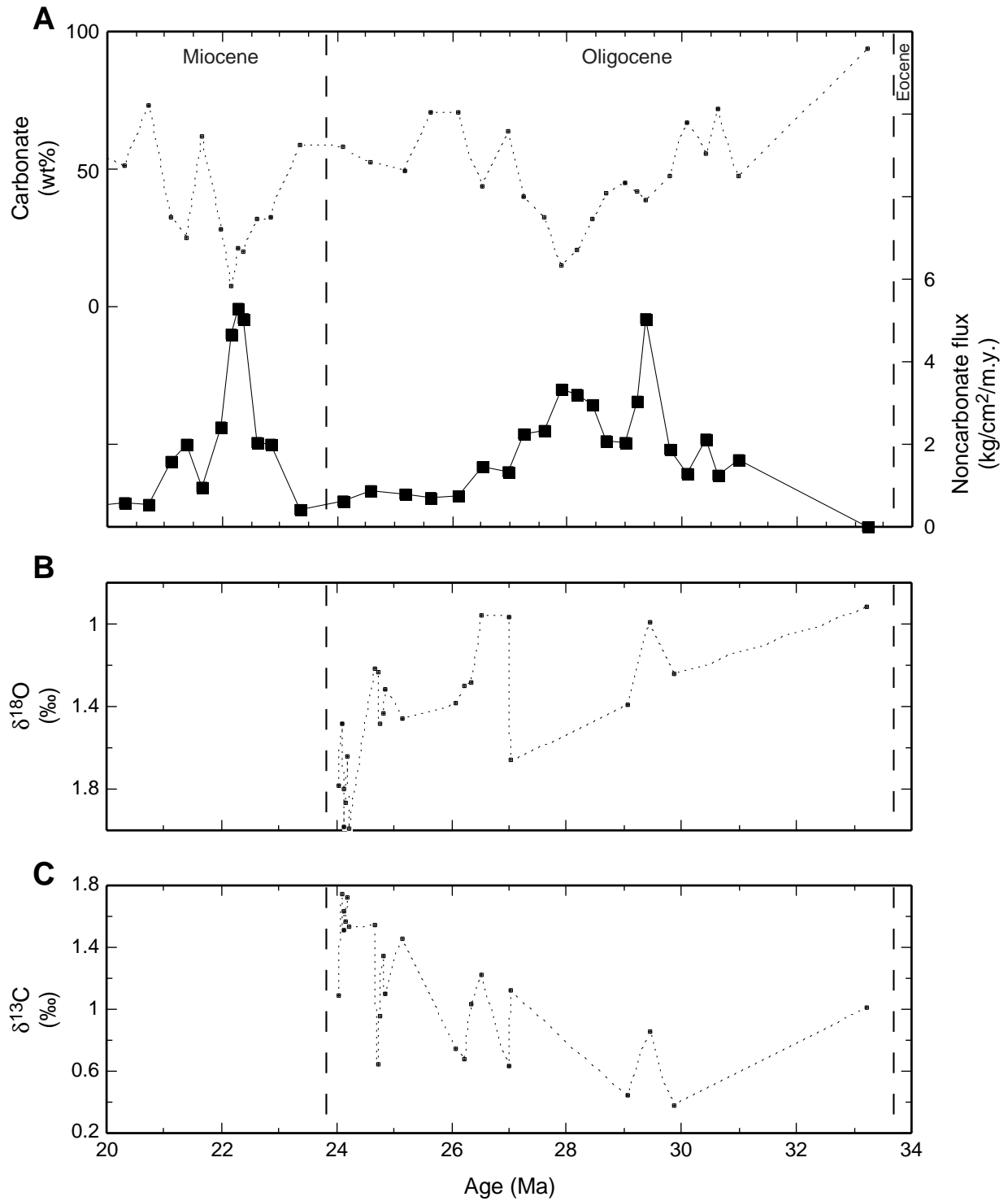
Table T1. Carbon, nitrogen, sulfur, and hydrogen analyses of sediments from Site 1139. (**See table notes.** Continued on next page.)

Core, section	Depth (mbsf)	CaCO₃ (wt%)	OC (wt%)	N (wt%)	S (wt%)	H (wt%)
183-1139A-						
1R-5	4.82	*64.06	0.24	0.03	BD	0.42
2R-3	13.42	*75.24				
3R-1	19.89	*73.61				
4R-1	29.39	*83.34	0.3	0.02	BD	0.17
5R-1	38.89	*76.32				
6R-1	48.39	*60.65				
7R-1	57.89	*51.33	0.15	0.05	0.14	0.34
8R-1	67.09	*72.89				
9R-2	77.23	*32.78				
10R-1	86.39	*24.94	0.36	0.06	0.38	0.42
11R-1	95.99	*62.13				
12R-1	105.59	*28.08				
13R-1	115.29	*7.46	0.25	0.05	0.41	0.36
14R-1	124.89	*21.19				
15R-1	134.39	*19.92				
16R-1	144.09	*31.99	0.18	0.03	BD	0.31
17R-1	153.69	*32.61				
18R-1	163.39	*58.51				
19R-1	172.99	*58.22	0.11	BD	0.15	0.16
19R-1	173.48	74.14				
19R-2	173.63	70.13				
19R-2	174.11	58.55				
19R-2	174.72	39.68	0.249	0.017		
20R-1	182.59	*52.78				
20R-2	183.87	35.17				
20R-2	184.39	38.80	0.167			
20R-3	185.42	55.45	0.1	0.013		
20R-4	187.15	61.27				
20R-5	187.89	61.82	0.136	0.013		
21R-1	192.19	*49.3				
21R-2	193.70	27.21				
21R-4	196.39	42.26	0.096			
21R-4	196.99	45.15				
21R-5	198.57	67.91				
22R-1	201.79	*70.91	0.03	BD	BD	0.2
23R-1	210.69	73.04				
23R-1	211.39	*70.56				
23R-3	213.89	52.64				
23R-3	214.29	52.61	0.1	0.011		
23R-5	217.25	79.04				
23R-6	218.55	56.49				
24R-1	220.99	*44.09				
25R-1	230.69	*64.08	0.17	0.02	BD	0.24
25R-1	231.03	53.55				
25R-2	231.73	56.41				
25R-4	235.33	32.62				
25R-4	235.69	25.75	0.095			
26R-1	240.29	*39.75				
26R-2	241.25	32.35				
27R-1	249.99	*32.34				
27R-3	252.29	51.71				
27R-4	254.83	13.27	0.13			
27R-4	254.95	13.67				
28R-1	259.59	*14.83	0.11	0.01	0.27	0.52
28R-4	263.71	27.63	0.091			
28R-5	265.89	36.15	0.093			
29R-1	269.19	*20.41				
29R-3	271.73	28.20	0.068			
29R-4	272.87	24.71	0.078			
30R-1	278.79	*32.04				
30R-5	285.05	42.56				
30R-6	285.75	22.67	0.083			
30R-6	285.75	22.67	0.07			
31R-1	288.39	*41.23	0.13	0.02	BD	0.32
32R-1	297.99	*45.25				

Table T1 (continued).

Core, section	Depth (mbsf)	CaCO₃ (wt%)	OC (wt%)	N (wt%)	S (wt%)	H (wt%)
32R-6	304.71	35.02	0.109			
32R-6	305.39	54.01				
33R-1	307.69	*41.77				
33R-3	309.99	64.13				
33R-5	313.35	36.40	0.077			
34R-1	317.29	*38.54	0.2	0.02	BD	0.31
34R-2	318.65	39.33	0.053			
34R-2	319.25	37.51				
34R-6	323.97	60.65				
34R-6	324.41	56.52				
35R-6	333.30	28.78	0.077			
36R-1	335.67	36.62				
36R-1	336.29	*47.33				
36R-2	337.41	41.39	0.082			
37R-1	345.89	*66.7				
37R-4	348.37	64.81				
37R-4	348.97	54.50				
38R-3	356.92	*55.46	0.19	0.03	BD	0.3
38R-5	360.30	73.56				
38R-6	361.48	41.09				
38R-7	362.70	76.01				
38R-7	363.18	66.59				
39R-1	365.09	*71.62				
39R-2	365.73	49.78				
40R-1	374.99	*47.54				
40R-3	377.03	30.64	0.112			
40R-4	379.49	39.12				
40R-CC	382.32	*93.54	0.04	0.03	BD	0.03

Notes: An asterisk indicates shipboard analysis (Shipboard Scientific Party, 2000). BD = below detection limit. Reported depth is top of sample interval.

Table T2. Grain size, opal, major element oxide, and trace element data for Site 1139 Unit II sediments.

Hole:	1139A-	1139A-	1139A-	1139A-	1139A-	*1139A-	*1139A-	*1139A-	*1139A-	*1139A-
Core, section:	21R-2	21R-5	27R-4	38R-6	38R-7	23R-5	25R-1	25R-4	27R-3	30R-6
Interval (cm):	90–92	127–129	123–125	35–37	7–9	75–77	123–125	139–141	19–21	35–37
Depth (mbsf):	193.7	198.57	254.83	361.48	362.7	217.25	231.03	235.69	252.29	285.75
$CaCO_3$ (wt%)	27.21	67.91	13.27	41.09	76.01	79.04	53.55	25.75	51.71	22.67
OC (wt%)	—	—	0.13	—	—	—	—	0.095	—	0.076
Md (mm)	—	—	—	—	—	2.3	6	7.6	5.6	6.5
Opal (wt%)	—	—	—	—	—	2.26	1.48	3.82	2.13	4.11
Major element oxides (wt%):										
SiO_2	39.80	15.26	44.44	29.37	10.80	54.38	52.31	51.28	52.87	52.02
TiO_2	1.17	0.70	2.29	1.60	0.56	3.04	3.44	3.52	3.40	3.29
Al_2O_3	10.99	4.35	12.40	7.24	2.75	14.31	14.66	15.81	15.95	15.18
Fe_2O_3*#	6.37	2.60	9.96	6.29	1.99	10.54	11.82	11.19	10.32	11.63
MnO	0.05	0.05	0.06	0.05	0.07	0.06	0.06	0.07	0.07	0.08
MgO	2.15	1.19	3.17	4.45	1.21	2.35	3.21	3.65	2.35	3.14
CaO	16.62	38.54	10.44	25.67	43.39	2.24	3.34	4.07	3.23	6.12
Na_2O	3.45	1.89	3.34	2.19	0.86	3.81	4.12	3.92	4.03	3.55
K_2O	2.78	0.81	2.90	0.98	0.55	3.46	2.84	2.68	3.64	2.53
P_2O_5	0.25	0.22	0.49	0.28	0.13	0.42	0.43	0.42	0.46	0.37
LOI**	15.87	33.07	9.83	20.73	35.87	3.93	3.21	2.58	2.83	1.90
Total	99.49	98.67	99.32	98.86	98.17	98.53	99.43	99.19	99.14	99.79
Trace elements (ppm):										
Sn	4.2	<5.5	<6.7	<5.5	<4.2		15.5	<6.4	<7.9	<5.9
Nb	69.7	22.1	43.3	18.3	7.4		56	61.4	65.1	50.1
Zr	334.6	102.7	263.6	143.3	51.5		321.9	356.2	347	294.4
Y	17.3	12.2	21.5	12.3	8.7		18.8	15.6	17.8	15.7
Sr	807.7	1328.6	693.9	1106	1445.1		553.2	561.3	633.9	701.9
Rb	64.6	13.3	58.1	14.6	7.3		46.8	42.3	52.5	43.7
Pb	6.3	<5.9	<10.6	<5.6	<6.0		12.8	6.7	5.9	13.1
Ga	15.3	6.5	18.8	9.7	3.4		26.4	26.2	24.8	23.8
Zn	88.4	37.8	91.5	55.6	12.5		154.5	140.8	455.6	150.5
Ni	38.7	19.6	52.7	82.3	19.8		67	48.7	28.8	43.9
V	70	39.4	164.3	100.2	38.2		185.3	166.9	151.6	193.6
Cr	23	<20.3	49.3	111.7	<25.0		155.5	123.1	117.2	59.5
Ba	945.8	862.1	834.6	385.1	347.5		1631.1	1228.1	1450.2	907.1
Co	14.9	6.7	21.5	22.2	5.3		73.3	26.5	14.4	29.8

Notes: * = treated sample (carbonate and opal removed). Md = median grain size diameter. *# = total Fe as Fe_2O_3. ** = loss on ignition at 1025°C for 4 hr.

Table T3. X-ray diffraction results and carbonate contents ($CaCO_3$) for Hole 1139A, Unit II.

Core, section, interval (cm)	Depth (mbsf)	$CaCO_3$ (wt%)	Minerals
183-1139A-			
6R-1, 90	48.40	61	Calcite, sanidine, clay, (glauconite)
7R-1, 91	57.91	51	Calcite, sanidine, clay, (glauconite)
8R-1, 61	67.11	73	Calcite, clay, (sanidine)
9R-2, 90	77.24	33	Calcite, clay, sanidine, maghemite, pyrite, (glauconite)
10-1, 91	86.41	25	Calcite, clay, sanidine, maghemite, pyrite, (glauconite)
11R-1, 91	96.01	62	Calcite, clay, (sanidine)
12R-1, 92	105.61	28	Calcite, clay, sanidine, maghemite, pyrite, (glauconite)
13R-1, 92	115.31	7	Clay, sanidine, calcite, maghemite, pyrite, plagioclase?, quartz, (glauconite), **chlorite**
14R-1, 92	124.91	21	Calcite, clay, sanidine, maghemite, plagioclase?, (glauconite, pyrite, quartz)
15R-1, 92	134.41	20	Calcite, sanidine, clay, maghemite, plagioclase?,
16R-1, 92	144.11	32	Calcite, clay, sanidine, maghemite, plagioclase?, (glauconite, pyrite, quartz)
17R-1, 92	153.71	33	Calcite, sanidine, clay, maghemite, plagioclase?, (pyrite, glauconite)
18R-1, 92	163.41	59	Calcite, clay, sanidine
19R-1, 92	173.01	58	Calcite, clay, sanidine, feldspar?, (maghemite, pyrite), **montmorillonite?**
19R-1, 138	173.48	74	**Insignificant clays in acidified sample**
19R-2, 112	174.72	40	**Insignificant clays in acidified sample**
20R-1, 92	182.61	53	Calcite, clay, sanidine, maghemite, (plagioclase?)
21R-1, 92	192.21	49	Calcite, clay, sanidine, (glauconite)
22R-1, 92	201.81	71	Calcite, clay, (sanidine)
22R-CC		~70	
23R-1, 92	211.41	71	Calcite, clay, (sanidine)
24R-1, 92	221.01	44	Calcite, clay, sanidine, maghemite, (glauconite, pyrite)
25R-1, 92	230.71	64	Calcite, clay, (sanidine, glauconite)
26R-1, 92	240.31	40	Calcite, clay, sanidine, glauconite, (maghemite, pyrite)
27R-1, 92	250.01	32	Calcite, clay, sanidine, glauconite, maghemite, plagioclase?, (clinoptilolite, pyrite)
27R-3, 30	252.29	52	**Smectite**
27R-4, 135	254.95	14	**Insignificant clays in acidified sample**
28R-1, 92	259.61	15	Calcite, clay, sanidine, maghemite, glauconite, (pyrite, plagioclase?, quartz)
28R-CC		~30	
29R-1, 92	269.21	20	Calcite, clay, sanidine, maghemite, (pyrite, plagioclase?)
30R-1, 92	278.81	32	Calcite, clay, sanidine, maghemite, glauconite, (pyrite, plagioclase?)
31R-1, 92	288.41	41	Calcite, clay, sanidine, glauconite, (maghemite, clinoptilolite)
32R-1, 92	298.01	45	Calcite, clay, sanidine, maghemite, glauconite, (clinoptilolite, pyrite, plagioclase?)
33R-1, 92	307.71	42	Calcite, clay, sanidine, glauconite, (maghemite)
33R-3, 19	309.99	64	**Insignificant clays in acidified sample**
33R-5, 55	313.35	36	**Insignificant clays in acidified sample**
34R-1, 92	317.31	39	Calcite, sanidine, clay, glauconite, (maghemite plagioclase?)
36R-1, 92	336.31	47	Calcite, clay, sanidine, maghemite, (quartz, plagioclase?)
37R-1, 92	345.91	67	Calcite, clay, (sanidine, clinoptilolite)
38R-3, 31	356.93	55	Calcite, clay, sanidine, (pyrite, glauconite)
39R-1, 92	365.11	72	Calcite, pyrite, (clay, sanidine, clinoptilolite)
40R-1, 120	375.00	48	

Notes: Minerals listed in order of decreasing abundance. Minerals listed in parentheses are present only in trace amounts. Items in plain text are shipboard measurements (Shipboard Scientific Party, 2000). Items in bold are new measurements from this study.

Table T4. Oxygen and carbon isotope data from bulk carbonate, ODP Site 1139.

Core, section, interval (cm)	Depth (mbsf)	CaCO$_3$ (wt%)	OC (wt%)	δ^{13}C (‰)	δ^{18}O (‰)
183-1139A-					
34R-6, 7–9	323.97	60.65		1.85	0.280
				1.95	0.363
				1.96	0.006
34R-6, 51–53	324.41	56.52		1.97	0.263
				1.99	0.413
				2.10	0.347
35R-6, 95–97	333.30	28.78	0.077	1.77	0.093
				1.81	0.353
				1.68	0.692
36R-1, 27–29	335.67	36.62		1.92	0.132
				1.96	0.255
				2.01	0.474
36R-2, 51–53	337.41	41.39	0.082	1.67	0.190
				1.76	0.374
				1.91	0.590
37R-4, 35	348.37	64.81		1.85	0.400
				1.97	1.020
				1.86	0.742

Table T5. Benthic foraminifer presence/absence data, Hole 1139A. (Continued on next page.)

Core, section:	40R-CC	40R-5	40R-3	38R-7	38R-3	37R-2	36R-3	35R-7	34R-6	34R-1	33R-3	32R-3	30R-2	29R-3	28R-2	27R-6	27R-3	26R-1
Interval top (cm):		126	18	78	110	38	46	86	10	102	50	78	38	74	106	42	30	18
Interval bottom (cm):		130	22	82	114	42	50	90	14	106	54	82	42	78	110	46	34	22
Depth (mbsf):	383.5	381.08	377	363.43	357.75	346.9	338.88	334.73	324.02	317.44	310.32	300.9	279.8	272.06	261.28	257.04	252.42	239.6
Alabamina sp.																		
Anomalinoides spissiformis																		
Anomalinoides pseudogrosserugosus				X				X										
Anomalinoides semicribratus																		
Bulimina impendens				X			X						X					
Bulimina macilenta							X			X			X					
Bulimina tuxpamensis				X														
Cibicides sp.		X																
Cibicidoides bradyi																	X	
Cibicidoides dickersoni												X	X					
Cibicidoides eocaenus																		
Cibicidoides grimsdalei																		
Cibicidoides havanensis		X																
Cibicidoides mexicanus																		
Cibicidoides micrus		X																
Cibicidoides mundulus																		
Cibicidoides praemundulus				X			X		X				X			X	X	
Hanzawaia ammophila																		
Laticarinina pauperata										X			X					
Nonion havanensis				X										X				
Osangularia mexicana							X						X					
Planulina costata								X										
Planulina renzi																		
Sphaeroidina bulloides								X										
Uvigerina mexicana																		
Uvigerina spinulosa																	X	
Pleurostomella spp.																	X	
Melonis barleeanum								X										
Uvigerina havanensis																		
Pseudononion sp.														X	X			
Astrononion pusillum				X									X			X	X	
Nuttallides umbonifera													X					
Eggerella bradyi													X					
Gyroidinoide sp.		X																
Globocassidulina subglobosa		X																

Note: X = present.

Table T5 (continued).

Core, section:	25R-3	25R-2	24R-1	23R-6	23R-5	23R-3	23R-1	22R-1	21R-5	21R-2	21R-1	20R-5	20R-4	20R-4	20R-4	20R-3	20R-2
Interval top (cm):	106	79	119	131	78	90	46	58	54	138	66	34	135	98	13	50	83
Interval bottom (cm):	110	83	123	135	82	94	50	62	58	142	70	38	137	102	17	54	87
Depth (mbsf):	233.88	232.1	221.3	219.32	217.3	214.42	210.98	201.5	197.85	194.2	191.98	188.06	187.58	187.21	186.36	185.2	184.04
Alabamina sp.			X		X	X	X					X			X	X	
Anomalinoides spissiformis												X					
Anomalinoides pseudogrosserugosus																	
Anomalinoides semicribratus											X	X		X			
Bulimina impendens																	
Bulimina macilenta												X				X	
Bulimina tuxpamensis																	
Cibicides sp.																	
Cibicidoides bradyi													X			X	
Cibicidoides dickersoni								X			X						
Cibicidoides eocaenus								X								X	
Cibicidoides grimsdalei										X							
Cibicidoides havanensis																	
Cibicidoides mexicanus								X				X		X		X	
Cibicidoides micrus																	
Cibicidoides mundulus												X	X		X	X	X
Cibicidoides praemundulus	X	X	X		X	X	X										
Hanzawaia ammophila										X							
Laticarinina pauperata	X		X									X		X	X	X	
Nonion havanense	X											X		X	X		
Osangularia mexicana					X							X	X		X		
Planulina costata																	
Planulina renzi										X				X		X	
Sphaeroidina bulloides					X	X										X	
Uvigerina mexicana										X		X					
Uvigerina spinulosa							X			X		X		X	X	X	
Pleurostomella spp.						X						X		X			
Melonis barleeanum								X	X			X		X	X		
Uvigerina havanensis												X					
Pseudononion sp.						X						X					
Astrononion pusillum	X	X	X	X								X					
Nuttallides umbonifera			X														
Eggerella bradyi																	
Gyroidinoide sp.																	
Globocassidulina subglobosa																	

Table T6. Oxygen and carbon isotope data from benthic foraminifers, ODP Site 1139.

Core, section, interval (cm)	Depth (mbsf)	Species	$\delta^{13}C$ (‰)	$\delta^{18}O$ (‰)
183-1139A-				
19R-1, 34–38	172.44	*Cibicidoides*	1.09	1.78
19R-1, 96–100	173.06	*Cibicidoides*	1.75	1.48
19R-1, 122–126	173.32	*Cibicidoides*	1.51	1.80
19R-1, 144–148	173.54	*Cibicidoides*	1.63	1.98
19R-2, 23–27	173.83	*Cibicidoides*	1.57	1.87
19R-2, 79–83	174.39	*Cibicidoides*	1.72	1.64
19R-2, 143–147	175.03	*Cibicidoides*	1.53	1.99
20R-2, 82–86	184.04	*Cibicidoides*	1.55	1.22
20R-3, 50–54	185.20	*Cibicidoides*	0.65	1.23
20R-4, 13–18	186.36	*Cibicidoides*	0.96	1.48
20R-4, 98–102	187.58	*Cibicidoides*	1.34	1.43
20R-5, 34–38	188.06	*Cibicidoides*	1.10	1.32
21R-1, 66–70	191.98	*Cibicidoides*	1.46	1.46
23R-1, 46–50	210.98	*Cibicidoides*	0.74	1.38
23R-3, 90–94	214.42	*Cibicidoides*	0.68	1.30
23R-5, 78–82	217.30	*Cibicidoides*	1.03	1.28
24R-1, 119–123	221.30	*Cibicidoides*	1.22	0.96
25R-2, 79–83	232.10	*Cibicidoides*	0.63	0.97
25R-3, 106–110	233.88	*Cibicidoides*	1.12	1.66
32R-3, 78–82	300.90	*Cibicidoides*	0.44	1.39
34R-6, 10–14	324.02	*Cibicidoides*	0.86	0.99
36R-3, 46–50	338.88	*Cibicidoides*	0.38	1.24
40R-CC	383.50	*Cibicidoides*	1.01	0.92

Table T7. Depths and ages of faunal, floral, and paleomagnetic criteria used to establish the chronology of Site 1139 and to calculate the sedimentation rates (Shipboard Scientific Party, 2000).

Core, section, interval (cm)	Datum	Type	Age (Ma)	Depth (mbsf)	Age
3R-CC	CN5a/CN3	Nannofossil	15–16	24	early middle Miocene
8R-CC	CN2–CN1	Nannofossil			mid-early Miocene
19R-CC	LO *Reticulofenestra bisecta*	Nannofossil	24	179.75	latest Oligocene
21R-CC	LO *Zygrhablithus bijugatus*	Nannofossil	26.2	200.25	late Oligocene
30R-CC	AP15–AP16	Foraminifer	28.5	275.45	late Oligocene
34R-CC	AP14	Foraminifer			"mid"-Oligocene
40R-6, 20–22	Above lower CP18	Nannofossil	<31	381.5	<early early Oligocene
40R-6, 89–91	Below CP16c	Nannofossil	>32.8	382.2	>late early Oligocene
40R-CC	CP16a/b	Nannofossil	32.8–34.3	384	Eocene–Oligocene

Notes: Age estimates of datum events are based on the timescale of Berggren et al., 1995. LO = last occurrence.

Table T8. Comparison of average terrigenous sediment and volcanic basement compositions, ODP Site 1139.

	Basement*	Sediment†	Change‡ (%)
Major element oxide (wt%):			
SiO_2	59.16	52.57	−11
TiO_2	2.15	3.34	55
Al_2O_3	15.54	15.18	−2
Fe_2O_3	9.96	11.10	11
MnO	0.20	0.07	−67
MgO	1.32	2.94	122
CaO	3.52	3.80	8
Na_2O	3.47	3.88	12
K_2O	4.16	3.03	−27
P_2O_5	0.74	0.42	−43
Trace element (ppm):			
Rb	72	46	−36
Ba	641	1304	104
Sr	228	613	169
Nb	100	58	−42
Zr	602	330	−45
Y	66	17	−74
V	139	174	26
Cr	18	114	545
Ni	4	47	983
Zn	191	225	18

Notes: * = mean of 23 basement analyses (Shipboard Scientific Party, 2000). † = mean of treated samples from this study. ‡ = 100 x (sediment − basement)/basement.